Elemental propagation of calcium signals in response-specific patterns determined by environmental stimulus strength

Helen Goddard*†, N. F. H. Manison*, D. Tomos†, and C. Brownlee*‡

*Marine Biological Association of the United Kingdom, The Laboratory, Citadel Hill, Plymouth PL1 2PB, United Kingdom; and †School of Biological Sciences, University of Wales, Bangor, Gwynedd LL57 2UW, United Kingdom

Communicated by Enid MacRobbie, University of Cambridge, Cambridge, United Kingdom, November 29, 1999 (received for review July 12, 1999)

Plant cells can respond qualitatively and quantitatively to a wide range of environmental signals. Ca^{2+} is used as an intracellular signal for volume regulation in response to external osmotic changes. We show here that the spatiotemporal patterns of hypo-osmotically induced Ca^{2+} signals vary dramatically with stimulus strength in embryonic cells of the marine alga *Fucus*. Biphasic or multiphasic Ca^{2+} signals reflect Ca^{2+} elevations in distinct cellular domains. These propagate via elemental Ca^{2+} release in nuclear or peripheral regions that are rich in endoplasmic reticulum. Cell volume regulation specifically requires Ca^{2+} elevation in apical peripheral regions, whereas an altered cell division rate occurs only in response to stimuli that cause Ca^{2+} elevation in nuclear regions.

Fucus | Ca^{2+} waves | Ca^{2+} sparks | inositol 1,4,5-trisphosphate | volume regulation

Plant growth and development in a fluctuating environment requires the ability to sense and respond, both qualitatively and quantitatively, to different stimuli. Ca^{2+} serves multiple roles as a second messenger (1), although the spatiotemporal patterns of Ca^{2+} signals, their mechanisms of propagation, and the ways in which specificity of response is encoded into appropriate downstream responses are poorly understood (1, 2). Both the vacuole (3, 4) and endoplasmic reticulum (ER) (5) have been implicated in the generation of physiologically significant Ca^{2+} signals in plants, although their relative roles in different signal-response pathways are uncertain. Whereas different magnitudes and temporal patterns of Ca^{2+} signal have been correlated with altered gene expression in animals and plants (6–9), the spatial patterns of environmentally induced Ca^{2+} signals underlying short-term physiological responses or longer-term regulation of gene expression remain poorly resolved. Moreover, the relative importance of nuclear (10) and cytoplasmic Ca^{2+} signals has not been studied in detail in any plant or algal cell type.

Transient elevations of Ca^{2+} following hypo-osmotic treatments have been reported in animals, yeast, algae, and higher plants (11–14). Both Ca^{2+} influx and intracellular release are involved in the generation of hypo-osmotic Ca^{2+} signals (11–14) that can vary in magnitude according to stimulus strength, although their spatial characteristics have not been characterized. Whereas propagating Ca^{2+} signals have been reported in plant cells in response to inositol 1,4,5-trisphosphate [$Ins(1,4,5)P_3$] (15) and electrical stimulation (16), the *Fucus* embryo provides one of the only examples among plants or algae of a Ca^{2+} wave as an essential signal arising in direct response to a physiological stimulus (13). Fucoid algae inhabit the intertidal zone and experience regular and dramatic changes in their external osmotic environment. They have thus evolved physiological mechanisms for regulation of cell volume and provide an ideal system for studying the mechanism of physiological Ca^{2+} signal propagation in plant cells.

Locally elevated Ca^{2+} is required in the growth zone of several polarized plant cell types (11–14, 17, 18). Two-celled *Fucus* embryos comprise a polarized growing rhizoid cell and a thallus cell. In their natural intertidal environment, they experience dramatic fluctuations in external osmotic conditions varying between extreme hypo- and hypersalinity. Hypo-osmotic treatment causes transient elevation of Ca^{2+} that is also initiated in the apical rhizoid region (13). Thus, osmotic Ca^{2+} signals are generated in the same cell region as the Ca^{2+} gradient involved in regulation of polarized growth, and it is not clear how responses of growth and osmoregulation to these Ca^{2+} signals are integrated.

To determine the spatiotemporal patterns of Ca^{2+} signals in response to different magnitudes of the same stimulus, we subjected two-celled *Fucus* embryos to varying degrees of hypo-osmotic shock. In addition, we compared downstream responses to Ca^{2+} signals that were generated in specific cell regions.

Materials and Methods

Plant Material and Dye Injection. *Fucus serratus* embryos were cultured to the two-celled stage in seawater (SW) for 24 h in unidirectional white light at 17°C as described (19, 20). Rhizoid cells were pressure microinjected with 10–50 μM concentrations of dye prepared in artificial cytoplasm solution (19, 20). Dyes used included fura-2-dextran (10 kDa), Calcium Green-dextran (10 kDa), or a mixture of Calcium Green-dextran and Texas Red-dextrans (10 kDa) (Molecular Probes).

Ca^{2+} Imaging. Fluorescence of injected cells was monitored at least 3 h after injection and recovery in SW. Photometric measurements of Ca^{2+} were made on fura-2-dextran-injected rhizoid cells (19, 20). For confocal imaging, zygotes were imaged after >3 h with a Bio-Rad (Hemel Hempstead, Hertfordshire, U.K.) 1024 confocal laser scanning microscope equipped with a Nikon ×40 (numerical aperture = 1.3) oil immersion lens and an argon/krypton laser. Cells injected with Calcium Green-dextran were imaged at 488 nm excitation and 522 nm emission, and those injected with Calcium Green/Texas Red-dextrans were excited simultaneously with 488 and 568 nm laser lines and emission monitored at 522 nm (for Calcium Green) and 605 nm (for Texas Red). Dark background was subtracted at each wavelength before image acquisition. In all cases, cell autofluorescence accounted for less than 10% of the minimum dye fluorescence values. Fluorescence sections (normally 20 lines × 512 pixels; 100 ms per section) and single confocal line scans (2 ms per line) of Calcium Green fluorescence, along the longitudinal axis of the rhizoid of injected zygotes were obtained with Bio-Rad TIME

Abbreviations: ER, endoplasmic reticulum; $Ins(1,4,5)P_3$, inositol 1,4,5-trisphosphate; SW, seawater.

‡To whom reprint requests should be addressed. E-mail: cbr@mba.ac.uk.

The publication costs of this article were defrayed in part by page charge payment. This article must therefore be hereby marked "*advertisement*" in accordance with 18 U.S.C. §1734 solely to indicate this fact.

Article published online before print: *Proc. Natl. Acad. Sci. USA*, 10.1073/pnas.020516397. Article and publication date are at www.pnas.org/cgi/doi/10.1073/pnas.020516397

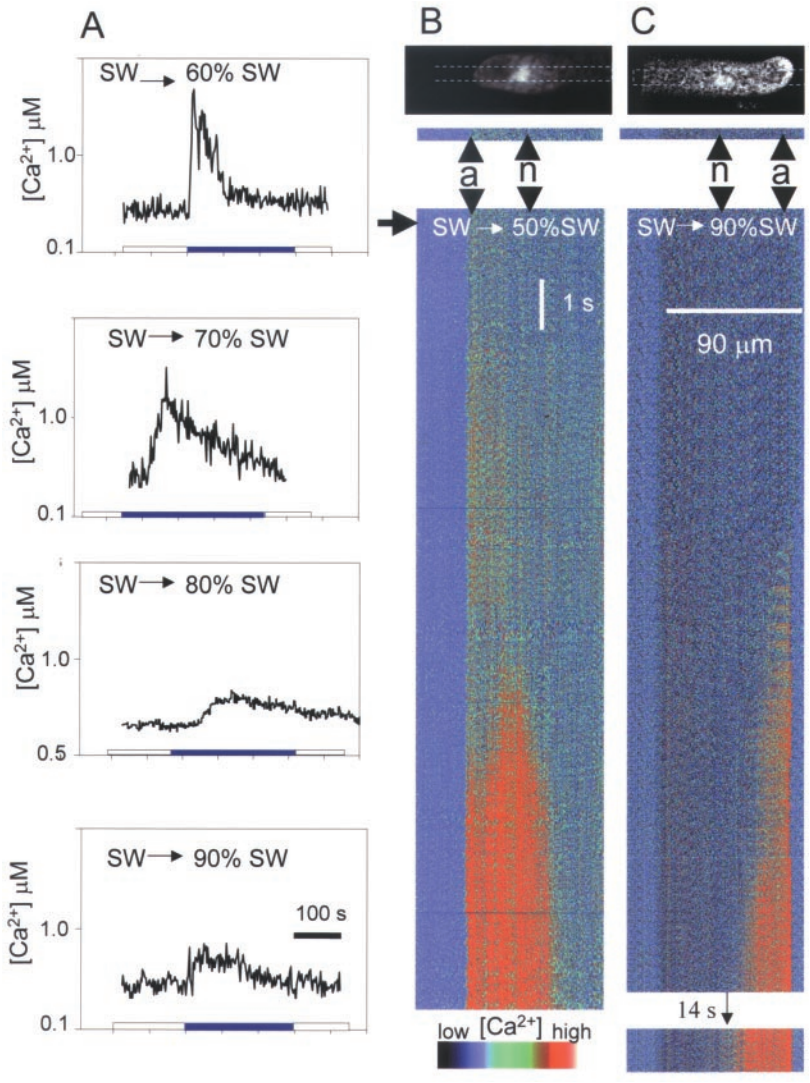

Fig. 1. Patterns of cytosolic Ca^{2+} signals in response to different degrees of hypo-osmotic shock. (*A*) Ratio photometric recordings of average global cell Ca^{2+} monitored with fura-2-dextran (13) in rhizoid cells in response to transfer from 100% SW to 60% ($n = 7$), 70% ($n = 20$), 80% ($n = 20$), or 90% ($n = 3$) SW. (*B* and *C*) Sequential plots of confocal sections (shown on the Calcium Green fluorescence images at the top of each plot) showing the relative increase in Calcium Green-dextran fluorescence in a rhizoid cell in response to transfer from 100% SW to 50% (*B*; $n = 26$) or 90% (*C*; $n = 7$) SW. Arrow indicates onset of osmotic treatment; *a* = cell apex; *n* = nuclear region. Confocal sections indicated were compiled sequentially to produce the pseudocolor temporal plots below each image.

COURSE software before and during hypo-osmotic Ca^{2+} signal generation.

Localized Ins(1,4,5)P_3 Photorelease. Rhizoid cells were microinjected with a mixture of Calcium Green-dextran and Texas Red-dextran (10 kDa, final intracellular concentrations of 10–50 μM) and caged Ins(1,4,5)P_3 (10 μM, Calbiochem). Localized photorelease of Ins(1,4,5)P_3 was achieved with a UV-pulsed nitrogen laser (10-ns pulses, 20 Hz, 1-s exposure; VSL 337; Laser Science, Cambridge, MA) delivered and focused to an adjustable spot size via a beam expander and adjustable focusing lens in the fluorescence port, delivery optics, and microscope objective. Laser intensity was adjusted with an adjustable diaphragm on the delivery optics to achieve photorelease. Calcium Green and Texas Red fluorescence were monitored simultaneously as described above.

Image Analysis. After acquisition, Calcium Green images were ratioed sequentially against an initial pretreatment image to give relative changes in dye fluorescence (F/Fo). The ratioed scans were spatially averaged with a 3×3 pixel window by using Kinetic Imaging (Liverpool, U.K.) Lucida software which calculates the average of the fluorescence values of a 3×3 pixel box and assigns the value to the pixel at the center of the box. Ratioed scans were displayed sequentially to form an image with the position along the rhizoid on the x axis and time on the y axis. For dual dye-injected zygotes, Calcium Green images were ratioed against the corresponding Texas Red image. Ca^{2+} concentrations were calculated from Calcium Green/Texas Red ratio values assuming elevation to saturating ratio values at the peak of the transient (13) and assuming a resting $[Ca^{2+}]$ of 139 nM measured in studies with fura-2 (13).

Line scans were displayed sequentially so that each image represents 1 s (512 lines). Three-dimensional plots were generated from these images by using Kinetic Imaging (Liverpool, U.K.) Lucida software. Statistical analysis of means, standard deviations, and variance of pixel values in a chosen area was performed before sequential ratio generation. The size and

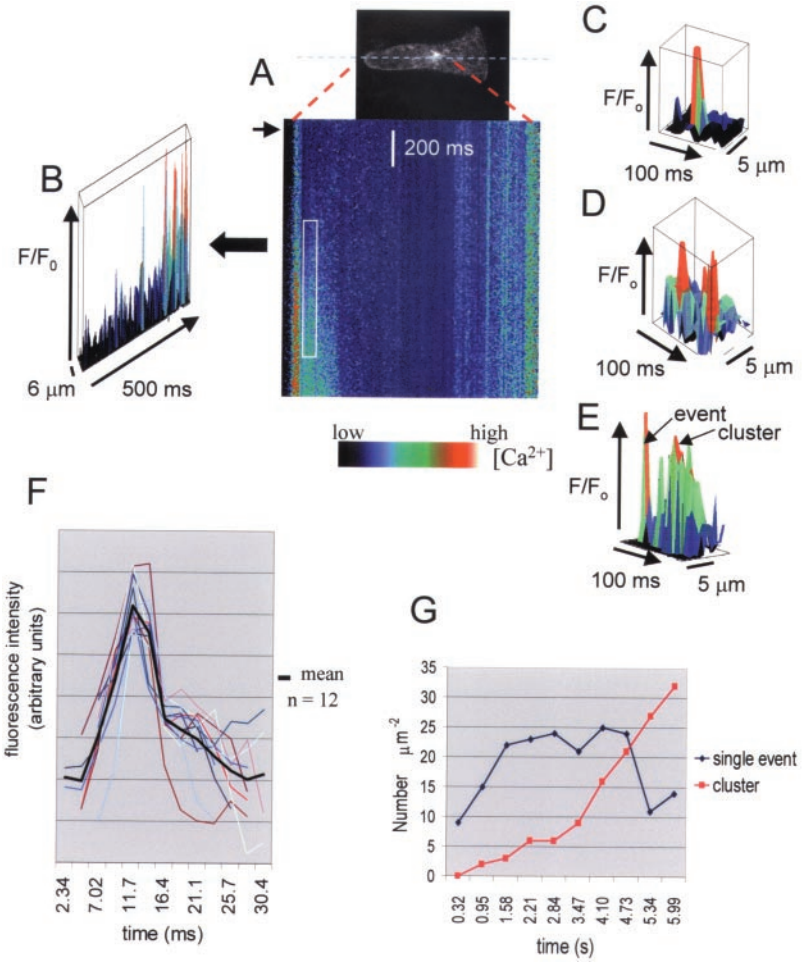

Fig. 2. Elemental Ca^{2+} elevations during Ca^{2+} wave propagation in a rhizoid cell. (*A*) Single-line confocal scans of Calcium Green fluorescence along the longitudinal axis of the cell during the initiation of Ca^{2+} waves are displayed sequentially to show the relative change in fluorescence following hypo-osmotic treatment [to 50% SW (arrow); $n = 25$.] The three-dimensional plot in *B* shows a nonuniform increase in Ca^{2+} during the onset of the Ca^{2+} wave in the rhizoid apex. In this plot, time increases from left to right whereas in the line-scan image (*A*), time increases from top to bottom. Elemental Ca^{2+} elevations in perinuclear regions (*C*) were frequently observed to arise repetitively at the same location (*D*). Events either occurred individually or appeared to cluster into more prolonged elevations (*E*). The data in *A–E* represent pixel values at least two SD of the background of a quiescent adjacent area (50 × 25 pixels). (*F*) Temporal profiles (colored plots) and averaged plot through elemental Ca^{2+} elevations show a rapid increase followed by a more gradual decline ($n = 12$). (*G*) The number of discrete elevations with values > 2 SD of the adjacent background at the rhizoid apex monitored over 630-ms time intervals increased initially during the first 1.5 s of wave propagation and then declined with the appearance of more prolonged elevations.

shape of the area analyzed (normally 20 × 20–50 pixels) was chosen to minimize variance of the Ca^{2+} signal because of the temporal increase in fluorescence intensity at the wave front. The occurrence of elemental events was identified by the increased variance/mean ratio of the calcium green fluorescence signal compared with the variance/mean ratio of a corresponding Ca-independent signal. Individual events were identified as having a fluorescence pixel value of >2 SD of background fluorescence intensity after 3 × 3 averaging.

Cell Division. Hypo-osmotic shocks of 15-min duration were administered to 24-h embryos at the two-cell stage. Cell numbers were counted after a further 12 h. Individual cells were visualized in confocal sections of embryos after incubation for 10 min with 1 μM fluorescent membrane dye FM1–43 (Molecular Probes).

Results and Discussion

The magnitude, duration, and pattern of hypo-osmotically induced cytosolic Ca^{2+} transients in the rhizoid cell strikingly depend on the magnitude of the stimulus (Fig. 1). Severe shocks (e.g., from 100% SW to 50% or 60% SW) induced an almost immediate rapid elevation of Ca^{2+} that declined within 100 s (Fig. 1*A*). This was characterized by an initial small transient elevation at the rhizoid apex that was followed, after 4–5 s, by an explosive Ca^{2+} increase initiating in the nuclear region that propagated bidirectionally at approximately 20 μm/s (80% of cells; Fig. 1*B*). This Ca^{2+} elevation was not excluded from the nucleoplasm. In the remaining 20% of cells, Ca^{2+} was seen to elevate in the nuclear region either before or simultaneously with the apical increase (Fig. 3*B*). In contrast to severe shocks, milder hypo-osmotic shocks (e.g., 100% SW to 90% SW) elicited Ca^{2+} elevations with a delayed onset (up to 60 s; Fig. 1 *A* and *C*) but which were significantly more prolonged. These were restricted to the rhizoid apex and did not propagate as Ca^{2+} waves.

Repetitive line scans along a longitudinal transect during the onset of hypo-osmotically induced Ca^{2+} waves revealed nonuniform Ca^{2+} elevations in highly discrete domains in both the rhizoid apex and perinuclear regions (Fig. 2 *A* and *B*). Individual events were spatially confined and lasted for 15–30 ms (mean = 24.9 ± 1.2, $n = 29$; Fig. 2 *C–F*), characterized by a rapid onset (duration 7–8 ms, mean = 7.2 ± 0.25, $n = 25$) and a slower decline (duration 17–20 ms; mean = 19.9 ± 1.4, $n = 25$). We

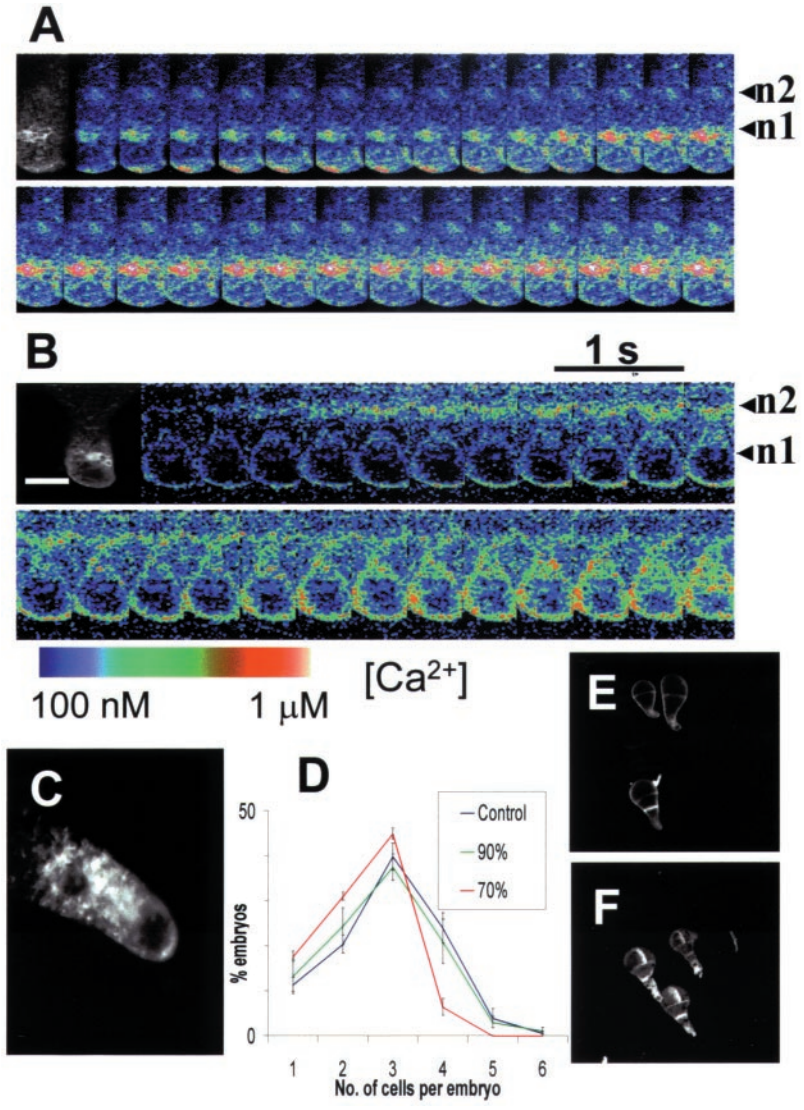

Fig. 3. Patterns of Ca^{2+} elevation following hypo-osmotic treatment in dividing cells. (*A*) Calcium Green to Texas Red ratio images during the onset of a hypo-osmotically induced Ca^{2+} wave (100% SW to 50% SW) shows an initial elevation of Ca^{2+} in the rhizoid apex which declines before the onset of Ca^{2+} elevation arising in the apical nucleus region ($n = 40$). (*B*) A variation in this pattern was evident in a minority of cells where Ca^{2+} elevations were observed to arise in subapical nucleus simultaneous with the apical Ca^{2+} elevation ($n = 10$). (*C*) Confocal sections of ER stained with 1.0 μM $DiOC_6$ (Molecular Probes) for 10 min show ER distributed in the rhizoid apex and perinuclear regions. (*D*) The number of cell divisions was significantly reduced following more severe hypo-osmotic shocks (e.g., 100% SW to 70% SW) that cause elevated nuclear Ca^{2+}. (*E* and *F*) Polarized rhizoid growth was unaffected by hypo-osmotic treatments up to 50% SW (*E*) compared with control untreated embryos (*F*). (Bar = 15 μm.)

estimate from the relative increase in Ca^{2+} dye fluorescence during unitary Ca^{2+} elevations that the amplitude of the events represents Ca^{2+} levels up to 200–300 nM above resting levels. However, analysis of event amplitude and frequency is complicated by the fact that not all events detected in a defined area necessarily originated in the region of interest or the plane of focus (21). There was no significant difference in the duration of apical and subapical events (25.0 ± 1.7 ms; $n = 9$ and 24.9 ± 1.5 ms; $n = 14$, respectively). During wave onset, the frequency of identifiable single events with amplitudes > 2 SD above the mean background level increased initially but declined as events became more clustered as the wave progressed (Fig. 2 *E* and *G*). In areas of sustained elevation, it was more difficult to discern individual events because of the increase in background Ca^{2+}. Unitary Ca^{2+} elevations were often observed to occur repetitively in the same domain (Fig. 2*D*) spatially separated by regions with fewer events and significantly lower variance to mean ratios of pixel intensity (two-tailed 1% significance level Wilcoxon test; $n_1 = 11, n_2 = 11$). Simultaneous line scans of Calcium Green and Texas Red fluorescence gave variance to mean ratios of pixel intensity at propagating wave fronts ranging from 3.1 to 10 (mean = 4.34, $n = 8$) for Calcium Green and from 0.77 to 2.17 (mean = 1.09, $n = 8$) for Texas Red fluorescence. There was no change in fluorescence of the Texas Red signal during wave progression (not shown). The significantly higher spatial variance of the Ca^{2+}-dependent fluorescence signal confirms that Ca^{2+} elevation occurred by increased frequency of spatially discrete elevations.

In rhizoid cells that had undergone nuclear division but not partition wall formation (Fig. 3), hypo-osmotically induced Ca^{2+} waves were observed to propagate from either of the two nuclear regions (Fig. 3). Most cells showed an initial transient elevation in the rhizoid apex followed by elevation in the apical nucleus (n1) spreading toward the subapical nucleus (n2) (Fig. 3*A*).

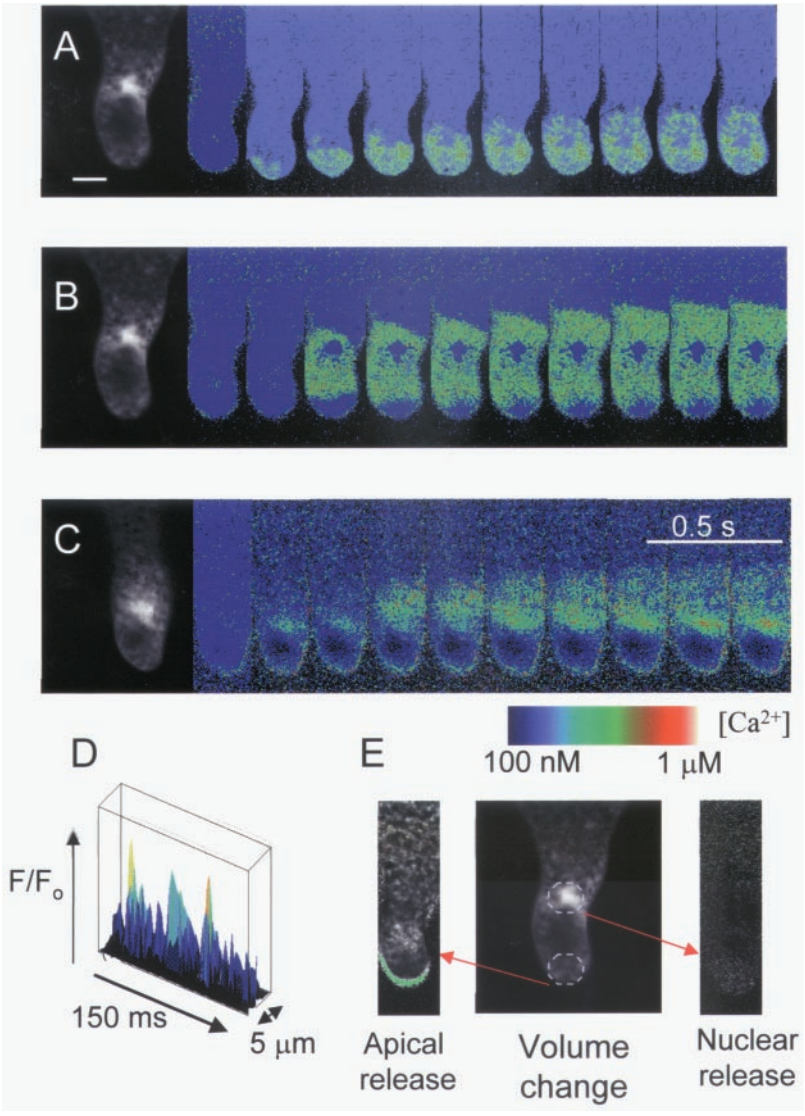

Fig. 4. Patterns of Ca^{2+} elevation in response to localized photorelease of caged Ins(1,4,5)P_3. (*A*) Photorelease of Ins(1,4,5)P_3 from a 10-μm diameter region at the rhizoid apex (*E*) caused Ca^{2+} elevation that propagated in a subapical direction but was generally (60% of cells, $n = 23$) restricted to the apical 40 μm. (*B*) Ins(1,4,5)P_3 release in the nuclear region induced a Ca^{2+} wave that propagated bidirectionally and did not permeate the nucleoplasm (8 out of 14 cells). (*C*) In a further six cells, Ca^{2+} release in the nuclear region gave an initial Ca^{2+} increase in the nucleoplasm followed by perinuclear Ca^{2+} waves. (*D*) Elemental Ca^{2+} elevations (>2 SD above the mean background) could be observed during propagation of Ins(1,4,5)P_3-induced Ca^{2+} waves in apical and subapical (not shown) regions. (*E*) Representative volume decrease in response to nuclear or apical Ins(1,4,5)P_3-induced Ca^{2+} elevations. The green area indicates volume decrease in a representative cell after release of caged Ins (1,4,5)P_3 in the apical rhizoid regions ($n = 5$). No volume decrease could be observed following Ins(1,4,5)P_3 release in nuclear regions. (Bar = 15 μm.)

However, in a minority of cells (20%), Ca^{2+} increased in the region of subapical nucleus either before, or simultaneous with, elevation at the rhizoid apex (Fig. 3*B*), followed by elevation in apical nucleus. Thus, the elevation of Ca^{2+} in the nuclear regions is not simply the result of a single propagating wave initiating at the rhizoid apex. The pattern of apical and perinuclear Ca^{2+} elevations correlated well with the observed distribution of ER (Fig. 3*C*). ER was prominent in the perinuclear region and at the cell apex but was only sparsely distributed in a chloroplast-rich region (not shown) 5–10 μM behind the rhizoid apex.

To determine the respective roles of Ca^{2+} signals in the apical and perinuclear regions, we monitored changes in rhizoid cell volume and rates of cell division following treatments that caused Ca^{2+} elevations in these regions. The cell division rate was influenced by different degrees of hypo-osmotic shock. Significantly fewer two-cell embryos subjected to hypo-osmotic treatments (from 100% SW into 70% SW or less) that caused nuclear Ca^{2+} signals, had progressed to the four-cell stage after 12 h compared with nonshocked embryos or those given treatments (from 100% SW into 90% SW) where Ca^{2+} elevations were restricted to the rhizoid apex (Fig. 3*D*). The response to more severe shocks was specific to cell division because rhizoid growth was unaffected by the hypo-osmotic treatment (Fig. 3 *E* and *F*).

Ca^{2+} elevations could be elicited in selected regions of the rhizoid cell by localized flash photolysis of caged Ins(1,4,5)P_3 (Fig. 4). This suggests a role for Ins(1,4,5)P_3 in the generation of Ca^{2+} signals in this system but does not provide direct proof that Ins(1,4,5)P_3-generated Ca^{2+} signals underlie responses to osmotic treatments. Photorelease of Ins(1,4,5)P_3 in the rhizoid apex caused Ca^{2+} elevations that were restricted to this region (Fig. 4*A*). Release of Ins(1,4,5)P_3 in the nuclear region produced

Ca^{2+} elevations that propagated bidirectionally through the perinuclear region (Fig. 4*B*) but did not propagate to the extreme rhizoid apex (Fig. 4 *B* and *C*). In most cells (80%), intranuclear Ca^{2+} remained essentially unchanged in response to Ins(1,4,5)P_3 photorelease. However, in a minority of cells (20%), Ins(1,4,5)P_3-induced Ca^{2+} elevation was also observed to occur within the nucleoplasm (Fig. 4*C*). Thus, in contrast to the osmotically induced nuclear Ca^{2+} signal that was not excluded from the nucleus, the Ins(1,4,5)P_3-induced Ca^{2+} elevation did not necessarily permeate the nucleoplasm, suggesting the involvement of factors additional to cytosolic Ins(1,4,5)P_3-induced Ca^{2+} release during hypo-osmotic signaling. The nuclear envelope may thus form a barrier to diffusion of Ca^{2+} or Ins(1,4,5)P_3 released in the perinuclear cytoplasm. Altered permeability of the nuclear envelope during the cell cycle (22, 23) could account for differences in nuclear Ca^{2+} observed in response to Ins(1,4,5)P_3-induced Ca^{2+} elevations.

Line scans of Ca^{2+} elevations in response to photorelease of Ins(1,4,5)P_3 revealed the presence of unitary Ca^{2+} elevations at the wave front (Fig. 4*D*). Ins(1,4,5)P_3 events and osmotically induced events did not differ significantly in amplitude, spatial dimensions (diameter at half-maximum amplitude: 2.11 $\pm$ 0.1 μm, $n = 13$ and 2.23 $\pm$ 0.1 μm, $n = 13$, respectively), rise rate/fall rate ratio (2.36, $n = 10$ and 2.41, $n = 15$, respectively), and duration (27.7 $\pm$ 1.2 ms, $n = 10$ and 24.9 $\pm$ 1.2 ms, $n = 10$, respectively). Comparison of cell volume before and after generation of Ins(1,4,5)P_3-induced Ca^{2+} transients showed that Ca^{2+} elevations at the rhizoid apex, but not those in the nuclear regions, resulted in cell volume decrease (Fig. 4*E*).

The occurrence of different Ca^{2+} signaling patterns in clearly defined cellular domains in response to a graded stimulus provides new insights into the generation of specificity of responses. The Ca^{2+} signal at the rhizoid apex is essential for turgor and volume regulation (13) and probably involves the regulation of ion channels that allow osmoregulatory ion efflux (24). Polarized growth requires localized Ca^{2+} elevation, transduced via Ca^{2+}/calmodulin (25, 26), regulation of targeted exocytosis (27), and a functional cytoskeleton (28). Studies with the Mn^{2+} quench technique revealed a role for Ca^{2+} influx in the generation of Ca^{2+} signals in the rhizoid apex (13). In the present study, the detection of elemental Ca^{2+} elevations within the cortical cytoplasm invokes an additional contribution from intracellular Ca^{2+} release in regulation of Ca^{2+} in this region. We also show here that nuclear Ca^{2+} signals elicited in response to more severe hypo-osmotic treatment regulate a different set of downstream responses. Thus, alterations in the cell division rate occurred only when there was a Ca^{2+} elevation in the nuclear region. This has parallels with yeast where hypo-osmotic Ca^{2+} transients monitored with aequorin luminescence correlate with inhibition of G2-M transition via activation of the mitogen-activated protein kinase MPK1 and calcineurin (29).

Whereas it is clear that the vacuole can serve as a Ca^{2+} source during intracellular signaling in plants (3, 4), this demonstration of propagating Ca^{2+} waves in ER-rich regions containing no significant vacuoles indicates the involvement of ER Ca^{2+} stores in these signals. In pollen tubes, discrepancy between the position of major vacuoles and the location of Ca^{2+} signals, elicited by photorelease of caged Ins(1,4,5)P_3, also suggested the involvement of nonvacuolar Ca^{2+} stores (30). The present study provides evidence that Ca^{2+} elevations propagate as unitary increases that have not been reported in nonanimal cells and which meet the criteria for elemental Ca^{2+} release from single channels or groups of channels in the ER (31–37). Moreover, the demarcation of osmotic Ca^{2+} signals to specific domains according to the strength of the stimulus indicates that Ca^{2+} release may be regulated differently in apical and perinuclear regions. This could reflect differences in the spatial distribution of Ins(1,4,5)P_3 receptor channels, functional characteristics of Ins(1,4,5)P_3 receptors, or specific regulatory factors in different regions. This may explain the occurrence of both graded volume regulation and qualitatively different longer-term responses arising from varying degrees of osmotic stimuli.

This work was supported by the Biotechnology and Biological Sciences Research Council, U.K. (N.F.H.M. and C.B.) and the Natural Environment Research Council, U.K. (C.B.). A University of Wales William Roberts Ph.D. studentship was awarded to H.G.

1. Sanders, D., Brownlee, C. & Harper, J. F. (1999) *Plant Cell* **11,** 691–706.
2. McAinsh, M. R. & Hetherington, A. M. (1998) *Trends Plant Sci.* **3,** 32–35.
3. Allen, G. J., Muir, S. R. & Sanders, D. (1995) *Science* **268,** 735–737.
4. Allen, G. J. & Schroeder, J. I. (1998) *Trends Plant Sci.* **3,** 123–125.
5. Muir, S. R. & Sanders, D. (1997) *Plant Physiol.* **114,** 1511–1521.
6. Knight, H., Trewavas, A. J. & Knight, M. R. (1997) *Plant J.* **12,** 1067–1078.
7. Dolmetsch, R. E., Lewis, R. S., Goodnow, C. C. & Healy, J. I. (1997) *Nature (London)* **386,** 855–858.
8. Gu, X. & Spitzer, N. C. (1995) *Nature (London)* **375,** 784–787.
9. Li, W. H., Llopis, J., Whitney, M., Zlokamik, G. & Tsien, R. Y. (1998) *Nature (London)* **392,** 936–941.
10. Ehrhardt, D. W., Wais, R. & Long, S. R. (1996) *Cell* **85,** 673–681.
11. Altamirano, J., Brodwick, M. S. & Alvarez-Leefmans, F. J. (1998) *J. Gen. Physiol.* **112,** 145–160.
12. Batiza, A. F., Schulz, T. & Masson, P. H. (1996) *J. Biol. Chem.* **271,** 23357–23362.
13. Taylor, A. R., Manison, N. F. H., Fernandez-Cruz, C., Wood, J. & Brownlee, C. (1996) *Plant Cell* **8,** 2015–2031.
14. Takahashi, K., Isobe, M., Knight, M. R., Trewavas, A. J. & Muto, S. (1997) *Plant Physiol.* **113,** 587–594.
15. Franklin-Tong, V. E., Drobak, B. K., Allan, A. C., Watkins, P. A. C.& Trewavas, A. J. (1996) *Plant Cell* **8,** 1305–1321.
16. Grabov, A. & Blatt, M. R. (1997) *Planta* **201,** 84–95.
17. Rathore, K. S., Cork, R. J. & Robinson, K. R. (1991) *Dev. Biol.* **148,** 612–619.
18. Miller, D. D., Callaham, D. A., Gross, D. J. & Hepler, P. K. (1992) *J. Cell Sci.* **101,** 7–12.
19. Roberts, S. K., Gillot, I. & Brownlee, C. (1994) *Development (Cambridge, U.K.)* **120,** 155–163.
20. Taylor, A. R. & Brownlee, C. (1992) *Plant Physiol.* **99,** 1686–1688.
21. Pratusevich, V. R. & Balke, C. W. (1996) *Biophys. J.* **71,** 2942–2957.
22. Feldherr, C. M. & Akin, D. (1990) *J. Cell Biol.* **111,** 1–8.
23. Lipp, P., Thomas, D., Berridge, M. J.& Bootman, M. D. (1997) *EMBO J.* **16,** 7166–7173.
24. Brownlee, C., Goddard, H., Hetherington, A. M. & Peake, L.-A. (1999) *J. Exp. Bot.* **50,** S1001–S1011.
25. Love, J., Brownlee, C. & Trewavas, A. J. (1997) *Plant Physiol.* **115,** 249–261.
26. Robinson, K. R. (1996) *Planta* **198,** 378–384.
27. Shaw, S. L.& Quatrano, R. S. (1996) *Development (Cambridge, U.K.)* **122,** 2623–2630.
28. Kropf, D. L. (1997) *Plant Cell* **9,** 1011–1020.
29. Mizunuma, M., Hirata, D., Miyahara, K., Tsuchiya, E. & Miyakawa, T. (1998) *Nature (London)* **392,** 303–306.
30. FranklinTong, V. E., Drobak, B. K., Allan, A. C., Watkins, P. A. C. & Trewavas, A. J. (1996) *Plant Cell* **8,** 1305–1321.
31. Klein, M. G., Cheng, H., Santana, L. F., Jiang, Y. H., Lederer, W. J. & Schneider, M. F. (1996) *Nature (London)* **379,** 455–458.
32. Song, L.-S., Stern, M. D., Lakatta, E. G. & Cheng, H. (1997) *J. Physiol. (London)* **505,** 665–675.
33. Bootman, M. D. & Berridge, M. J., (1995) *Cell* **83,** 675–678.
34. Lipp, P. & Niggli, E. (1996) *J. Physiol. (London)* **492,** 31–38.
35. Niggli, E. (1999) *Annu. Rev. Physiol.* **61,** 311–335.
36. Shirokova, N. & Rios, E. (1997) *J. Physiol. (London)* **502,** 3–11.
37. Parker, I. & Yao, Y. (1991) *Proc. R. Soc. London Ser. B* **246,** 269–274.